Technical Inspection Engineering

Iranian Journal of Oil & Gas Science and Technology, Vol. 6 (2017), No. 1 pp. 63-76
http://ijogst.put.ac.ir

Nanocomposite Coating Based on Thermoplastic Acrylic Resin and Montmorillonite Clay: Preparation and Corrosion Prevention Properties

Davood Jafari[1], Mohammadreza Shishesaz[2]*, Davood Zaarei[3], and Iman Danaee[2]

[1] M.S. Student, Department of Inspection Engineering, Petroleum University of Technology, Abadan, Iran
[2]Associate Professor, Department of Inspection Engineering, Petroleum University of Technology, Abadan, Iran
[3] Associate Professor, Department of Polymer Engineering, South Tehran Branch, Islamic Azad University, Tehran, Iran

Received: September 03, 2014; *revised:* November 19, 2014; *accepted:* December 07, 2014

Abstract

Different amounts of nanoclay were incorporated into the acrylic resin matrix at 0, 1, 3, and 5 wt.% loadings. The coatings were applied on low carbon steel plates. Optical microscopy, sedimentation test, transmission electron microscopy, and X-ray diffraction were employed to investigate the dispersion of nanoclay in matrix. The corrosion resistance of coatings was evaluated by electrochemical impedance spectroscopy, polarization measurement, and salt spray test. In addition, pull-off and cross-cut tests were used for the assessment of coating adhesion to the substrate. The results indicated that the anti-corrosive properties of the acrylic resin were obviously increased by the addition of nanoclay. The nanocomposite coatings containing 3 wt.% clay showed the best corrosion resistance. Finally, the nanocomposites containing 1 and 3 wt.% showed the highest adhesion to the substrate.

Keywords: Nanocomposite Coating, Montmorillonite, Corrosion, Impedance, Salt spray

1. Introduction

Organic coatings, along with proper surface pretreatment, are the most common and economical methods for the protection of metallic objects and structures against corrosion (Bierwagen, 1996). Organic coatings make a barrier by preventing the diffusion of oxygen, water, and aggressive ions. However, there is no perfect barrier coating, and all coatings eventually fail due to existing pinhole defects (Zaarei et al., 2008).

Several methods have been utilized to improve the corrosion resistance of coatings (Zhang et al., 2003; Ash et al., 2003). Using nanomaterials, especially nanoclay, is one of the most widely used methods for improving the mechanical and chemical properties of polymeric coatings (Zhou et al., 2002). In recent years, several authors studied on thermal/mechanical and chemical properties of polymer–clay nanocomposite coatings (Chen et al., 2005; Chen et al., 2003; Bagherzadeh et al., 2007; Sun et al., 2007;

* Corresponding Author:
Email: shishesaz@put.ac.ir

Solarski et al., 2005). Polymers such as polyaniline (Yeh et al., 2001), polypyrrole (Yeh et al., 2003), poly (methyl methacrylate) (Yeh et al., 2002; Chang et al., 2008), polyimide (Yu et al., 2004), polystyrene (Yeh et al., 2004), polyurethane (Chen et al., 2000), and epoxy (Ratna et al., 2003; Lan and Pinnavaia, 1994; Chang et al., 2008; Darmiani et al., 2013) along with nanoclay were widely used as polymer clay nanocomposite (PCN).

Polymer–layered silicate nanocomposites (PLSN) usually exhibit improved properties compared to pristine polymers and conventional composites (Xidas and Triantafyllidis, 2010). These improvements are related to the morphology of the layered silicates and structure of the nanoparticles in the polymer (Thi Xuan Hang et al., 2007). Polymer–clay nanocomposites, with fully-exfoliated platelet structure of nanoclay dispersed within a polymer matrix, provide excellent mechanical and barrier performances. This is due to the high surface-to-volume ratio of the nanofiller and the increased tortuosity of the diffusion pathways for oxygen, water, and aggressive ions, which decreased the permeability of these ions and improved the corrosion resistance of the resultant coatings (Sun et al., 2007)

The most widely used layered silicate is montmorillonite (MMT) (Thi Xuan Hang et al., 2007). As pure MMT is a hydrophilic phyllosilicate, it is only miscible with hydrophilic polymers. It is necessary to exchange alkali counter ions with cationic organic surfactants to improve the compatibility of MMT with organic monomer or polymers (Xiong et al., 2004). Different approaches can be employed to incorporate the ion-exchanged layered silicates into the polymer hosts such as in situ polymerization, solution intercalation, or simple melt mixing (Pavlidou and Papaspyrides, 2008).

The aim of this study is to obtain an appropriate formulation of acrylic–montmorillonite (MMT) nanocomposite coating. Clay particles were dispersed into acrylic by mechanical agitation and sonication processes. The dispersion morphology and degree of agglomeration were analyzed by sedimentation tests, X-ray diffraction (XRD), optical microscopy, and transmission electron microscopy (TEM). The anticorrosive properties of the nanocomposite coatings were evaluated by electrochemical impedance spectroscopy (EIS), polarization study, and salt spray tests. Pull-off adhesion tests were also employed to investigate the adhesion of coatings to substrate.

2. Experimental

2.1. Materials

The used nanoclay provided by Southern Clay Company (USA) was a dimethyl, dehydrogenated tallow, quaternary ammonium–modified montmorillonite (Cloisite 20A) with a particle size of 2–13 µm and a layer thickness of 1 nm. The acrylic resin derivatives (thermoplastic acrylic grade MP35) were supplied from Taak Resin Company. Typical properties of the acrylic resin are shown in Table 1. Xylene used as the solvent was provided from Isfahan Petrochemical Company.

Carbon steel sheets (150×10×2 mm) were used as metallic substrates subjected to a sequence of a solvent cleaning and mechanical surface polishing using emery papers from #120 to #800 to remove any trace of surface oxides. Then, the working sheets were kept in a desiccator. Prior to coating application, the plates were cleaned and dried with acetone.

Table 1
Typical properties of the used acrylic and acrylic/styrene resins.

Typical Properties	
Resin	Acrylic grade Mp-35

Appearance	Clear liquid
Type	Non crosslinking
Solvent	Xylene
Color (hazen)	<80
Color (gardner)	<1
Solids	(58±1)%
T_g	+37 °C
Viscosity at 25 °C	3000-6000 cP
Density at 25 °C	0.97 g/ml
Flash point	24 °C

2.2. Preparation of nanocomposites

The desired amount of resin and nanoclay were mechanically mixed at 1200 rpm for 90 minutes. Then, the mixture was subjected to sonication for 1 hr. using Hielscher Ultrasonics GmbH Co. UIP1000hd instrument. During the sonication process, the temperature of the mixture was controlled by putting the reaction vessel in an ice bath. Different nanocomposite mixtures containing 1, 3, and 5 wt.% organoclay were prepared.

2.3. Sample preparation

The prepared mixtures were applied on the carbon steel substrates using a film applicator with a wet film thickness of 60 μm. The samples were allowed to cure for 3 weeks at laboratory atmosphere. The dry film thickness (DFT) measured using Elcometer FN 4653 digital coating thickness meter (Elcometer Co. Ltd.) was about 30±3 μm.

2.4. Laboratory Tests

The Low-angle XRD was performed using X'Pert Pro MPD X-ray diffractometer by a copper target, at a flow intensity of 40 mA, at a voltage of 40 kV, and in a 2θ range of 0.5–10°. The interlayer spacing of the nanocomposites was derived from the peak position of d_{001} in the XRD diffractograms according to Bragg's equation ($n\lambda = 2d \sin(\theta)$). Transmission electron microscopy (TEM) was used to distinguish the dispersion of clay in polymer matrix using Philips CM30 300-kV high-resolution TEM.

The electrochemical impedance spectroscopy (EIS) measurement was carried out in a 3.5% NaCl solution at room temperature using AUTOLAB PGSTAT 302N instrument in the frequency range of 100 kHz–10 mHz, at open circuit potential, and at an AC amplitude of 10 mV. A conventional three-electrode cell with a saturated Ag/AgCl electrode as a reference and platinum counter electrode was used. The exposed surface area of working electrode was 3 cm^2. To evaluate the corrosion protection performance of the coating, the EIS measurements were conducted at different exposure times up to 45 days.

The polarization studies were done around the equilibrium potential (±300 mV) at a scan rate of 1 mVs^{-1}. The corresponding data were calculated using Tafel extrapolation method. The polarization resistance (R_p) was determined by Stern–Geary equation from the polarization measurements.

$$R_p = \frac{a.\ c}{2.303(\ a + \ c)} \times \frac{1}{I_{corr}} a \quad (1)$$

where, I_{corr} is the corrosion current density, and β_α and β_c represent the anodic and cathodic Tafel slope respectively.. The accelerated corrosion test was conducted in a salt spray chamber (B. AZMA CTS-114D, Iran) using a 5% NaCl solution for 720 hrs based to ASTM B-117.

2.5. Pull-off and cross cut adhesion test

The initial coating adhesion and the adhesion after removing the sample from the salt spray (fog) chamber were measured using a direct pull-off adhesion test method in accordance with ASTM D4541 type III (self-aligning adhesion tester).

A high viscosity cyanoacrylate adhesive (Cyanoacrylate MC1500) was used for bonding the dollies with an area of 0.5 cm^2 to the coating. In adhesion measurement after exposure, the samples were removed from the salt spray chamber, rinsed completely with distilled water ,and allowed to dry for 48 hrs at room temperature. The glued dollies were then allowed to dry at ambient temperature. A digital adhesion tester (Elcometer 108, Elcometer Co. England) was employed to ensure the reproducibility of the test area; all of the measurements were obtained from at least three experiments.

The crosscut adhesion test was accomplished according to ASTM D3359 by scratching parallel lines in both longitude and latitude directions on the coating using a scalpel. A standard adhesive tape was then applied to the surface and peeled off. The visual inspection of the tape is performed based on the amount of coating removed from the surface. Adhesion strength was rated according to a scale from 0B (the weakest) to 5B (the strongest).

3. Results and discussion

3.1. Stability

Figure 1 presents the suspension state of MMT in the acrylic resin. The mixture containing 5% nanoclay was formed by mechanical agitation and the sonication process. With increasing the temperature of mixture, the viscosity of the final mixture was decreased and sedimentation rate was increased. In the case of mechanically agitated dispersion, sediments could be seen at the bottom of test tube, while, by using sonication, no phase separation or sediment was observed. In fact, transfer of local shear stress in the sonication process broke down the aggregates of clay particles, which led to improving the dispersion.

3.2. Optical microscopy results

The samples containing different amounts of clay were observed using optical microscope. Figure 2a shows the mechanically agitated sample for 90 min which contain many MMT agglomerates. Figure 2b and 2c present the optical micrographs of 3 wt.% organoclay suspensions after 90 min mechanical agitation followed by sonication processes for 30 and 60min respectively. The results indicate that the dispersion of clay in matrix is improved by using an ultrasonic mixer.

Figure 1
Suspension of 5 wt.% organoclay/acrylic dispersions: a) after 90 min mechanical agitation, and b) after 90 min mechanical agitation and 1hr sonication.

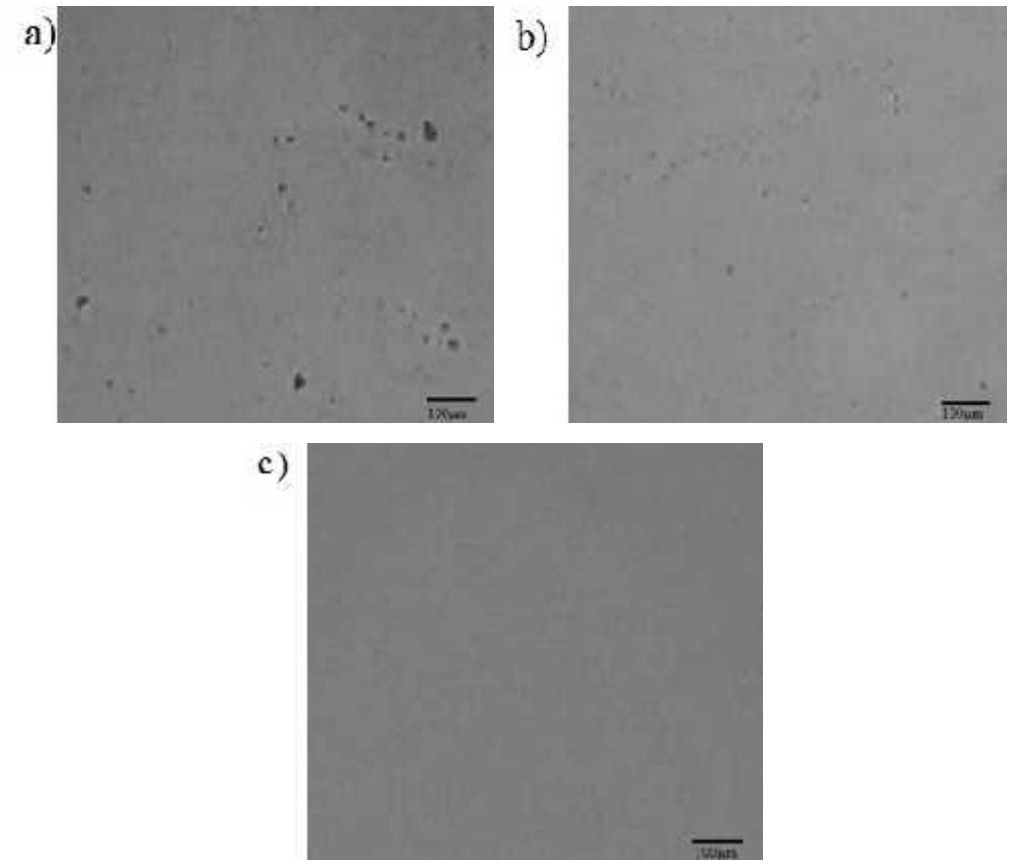

Figure 2
Optical micrographs of 3wt.% organoclay/acrylic suspensions: a) after 90 min mechanical agitation, b) after 30 min sonication, and c) after 60 min sonication.

3.3. XRD

The XRD studies were carried out on the pristine clay (closite20A) and the nanocomposites containing 1, 3, and 5 wt.% MMT to assess the degree of clay intercalation in the polymer film and the formation of the nanocomposites. As shown in Figure 3, the curve of Cloisite 20A presents a broad peak at 2θ=3.568°, which indicates that the *d*-spacing between two silicate layers is about 2.473 nm (calculated using the Bragg's law $d=\lambda/ [2 \sin (\theta)]$). Moreover, the *d*-spacing of clay were increased in the nanocomposite samples. The results of XRD pattern are shown in Table 2. An increase in the *d*-spacing of clay indicated that the acrylic molecules were intercalated into the MMT layers of the nanocomposites.

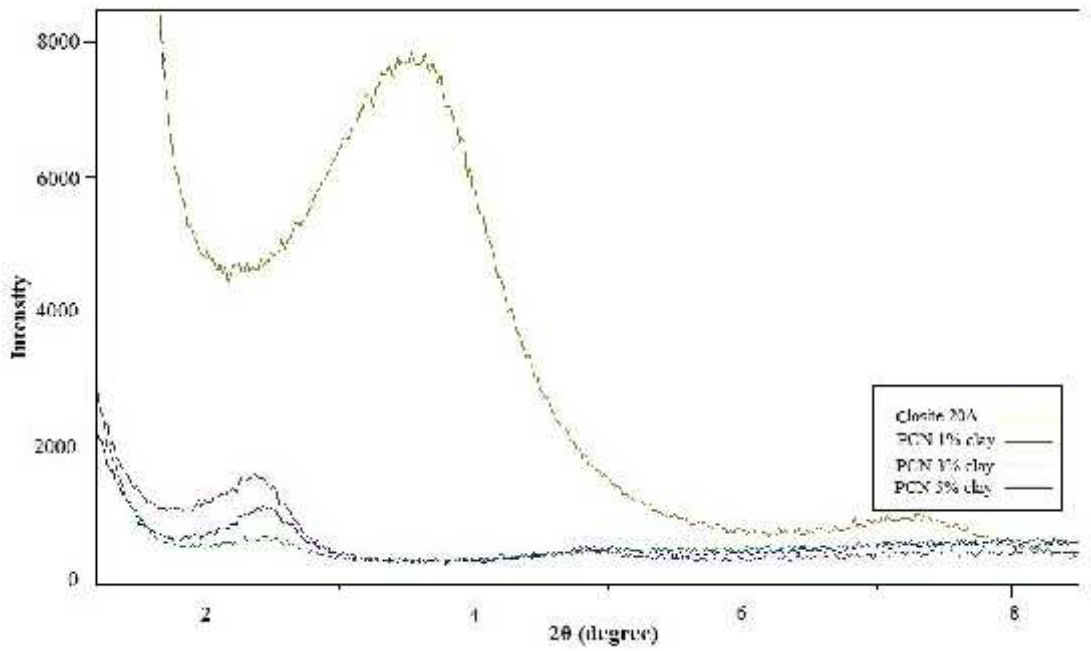

Figure 3
XRD patterns of Cloisite 20A and diffraction patterns of the acrylic–clay nanocomposite.

Table 2
XRD result of Cloisite 20A and diffraction patterns of the acrylic–clay nanocomposite.

Product	Typical diffraction peak (2θ)	Basal spacing (nm)
Cloisite 20A	3.568	2.473
PCN 1%	2.457	3.593
PCN 3%	2.445	3.6105
PCN 5%	2.375	3.700

3.4. TEM

The actual nature of a nanocomposite can be observed using TEM images. Figure 4 represents the TEM result of the nanocomposite containing 3 wt.% clay. It could be seen that the clay was partially exfoliated or intercalated in the acrylic matrix. The dark lines represent the sheets of Cloisite 20A with variable thicknesses from 1 to 6 nm (Ranade et al., 2002). The spaces between the dark lines represent the interlayer spaces (Zaarei et al., 2010). As shown in Figure 4, the structure of the nanocomposite

seems to be rather an intercalated structure. Platelet spacing indicated by the TEM images confirmed the trend of the XRD result.

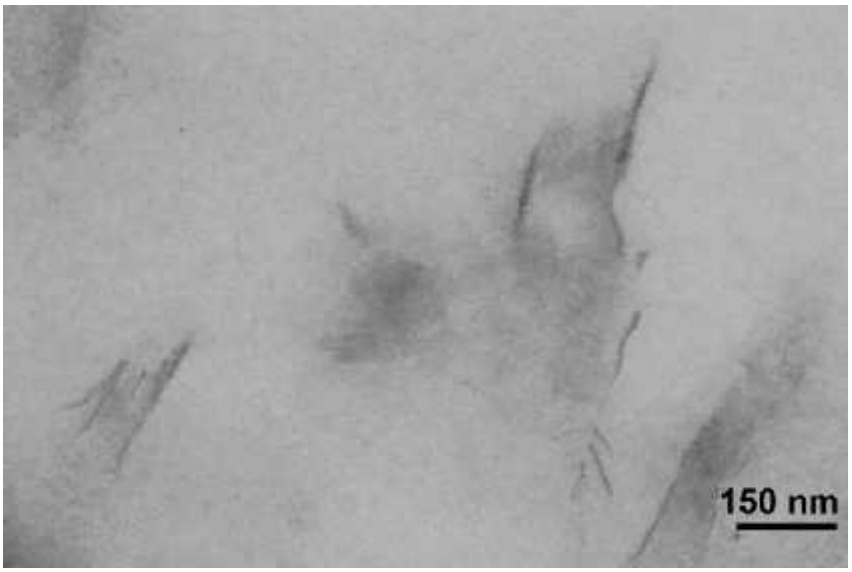

Figure 4
TEM micrographs of acrylic/3 wt.% clay nanocomposite.

3.5. Corrosion studies

3.5.1. Electrochemical impedance spectroscopy (EIS)

Bode plots of the EIS studies for the different coatings obtained at various immersion times in a 3.5 wt.% NaCl solution are presented in Figures 5-9. The addition of clay into the acrylic coatings caused an increase in the corrosion resistance during the long period of the immersion time. This means that the protection of the steel was increased by the use of the nanocomposite coatings.

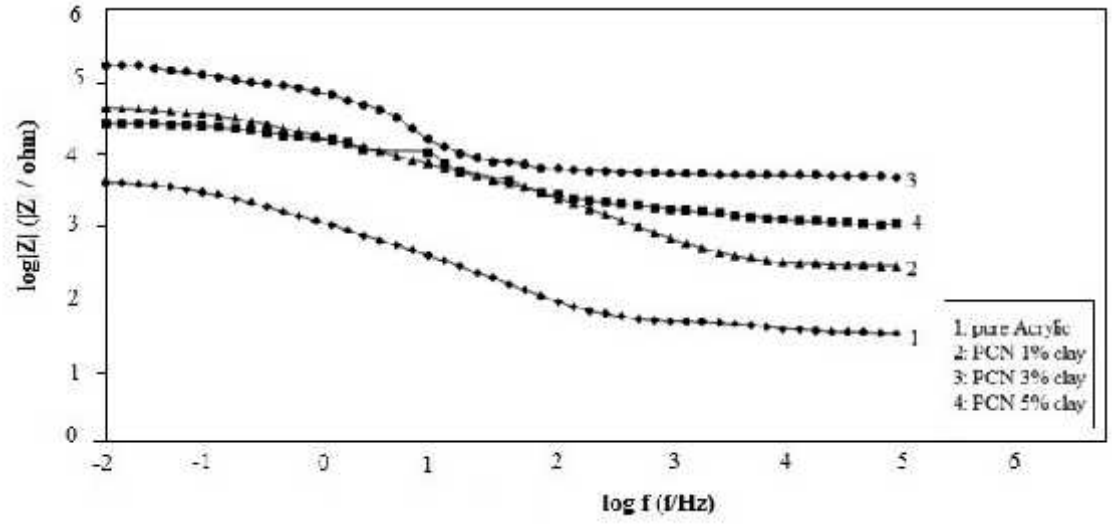

Figure 5
Bode plots of the EIS spectra for the different samples after 7 days of immersion in a 3.5 wt.% NaCl solution.

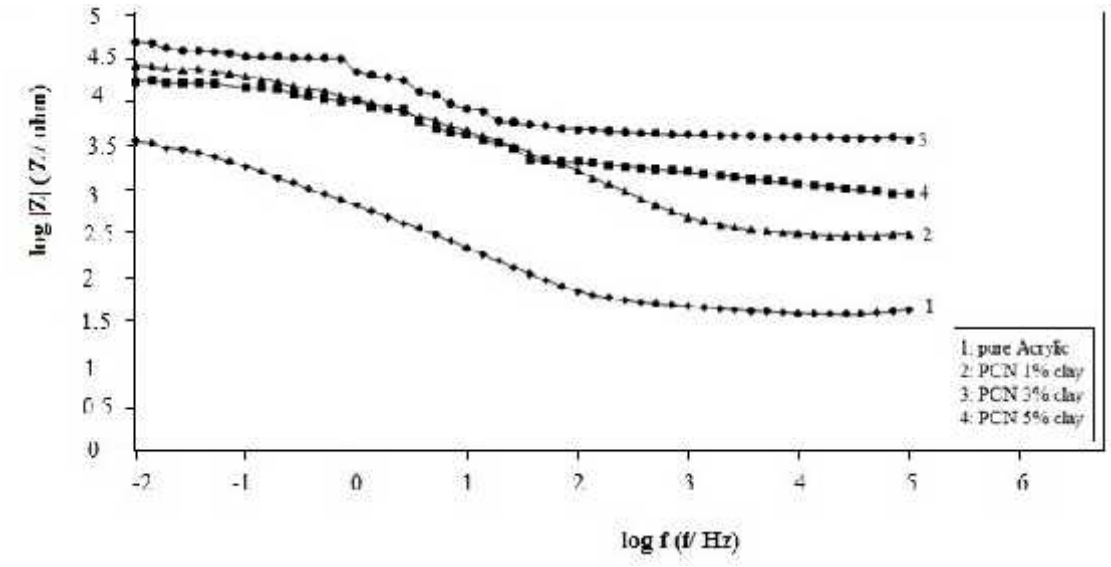

Figure 6
Bode plots of the EIS spectra for the different samples after 15 days of immersion in a 3.5 wt.% NaCl solutions.

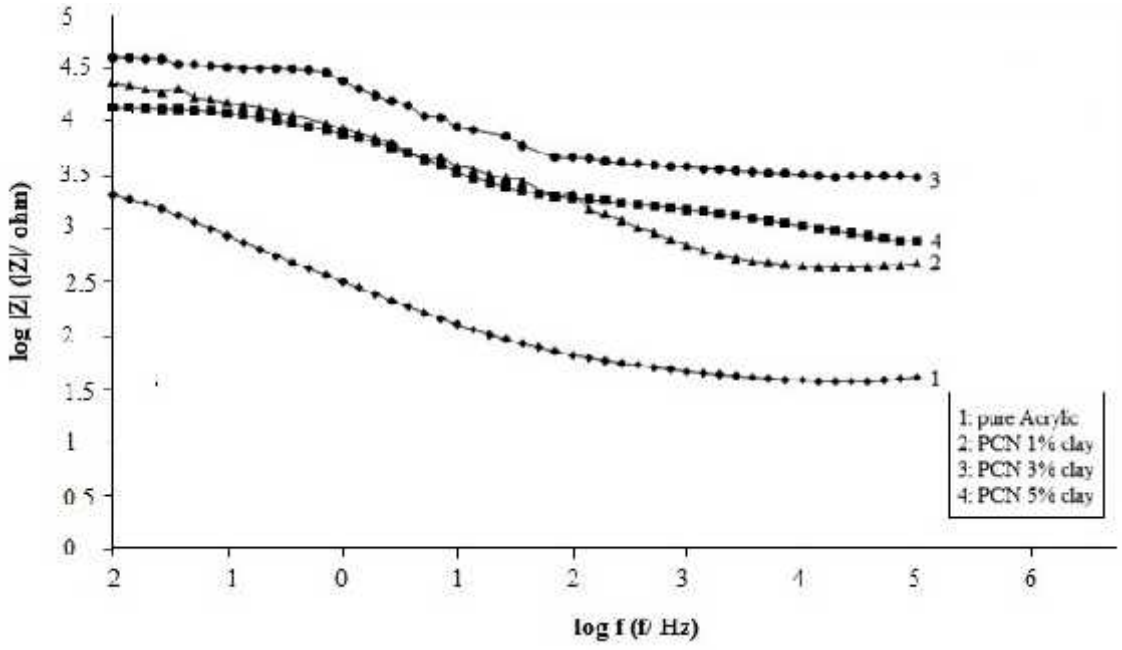

Figure 7
Bode plots of the EIS spectra for the different samples after 28 days of immersion in a 3.5 wt.% NaCl solution.

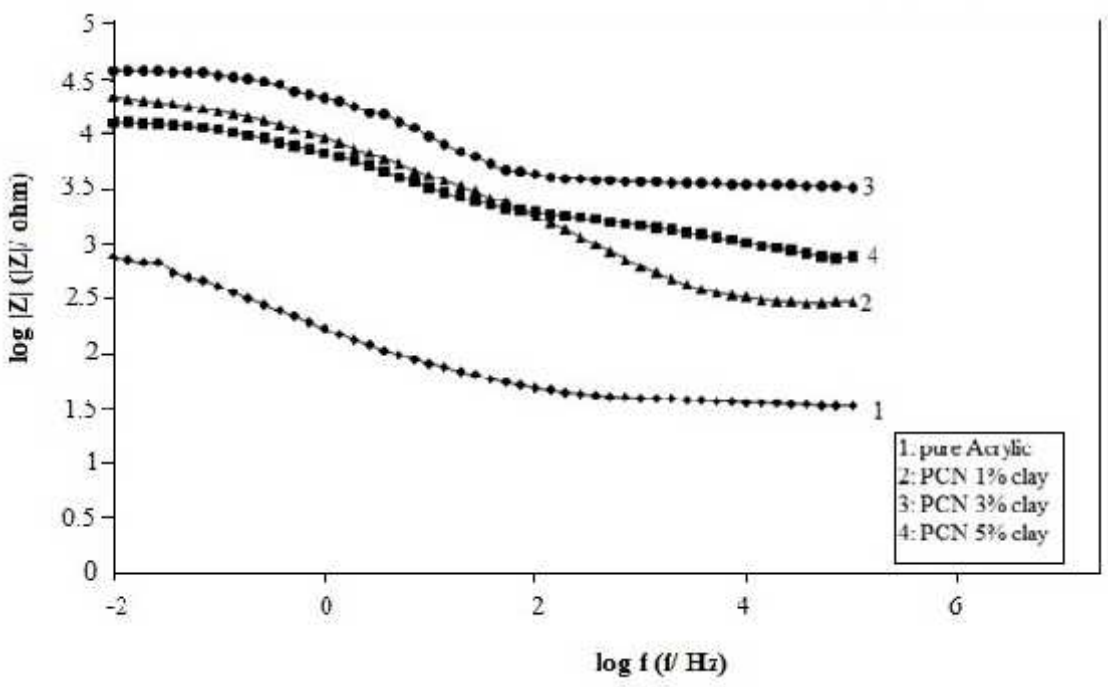

Figure 8
Bode plots of the EIS spectra for the different samples after 36 days of immersion in a 3.5 wt.% NaCl solution.

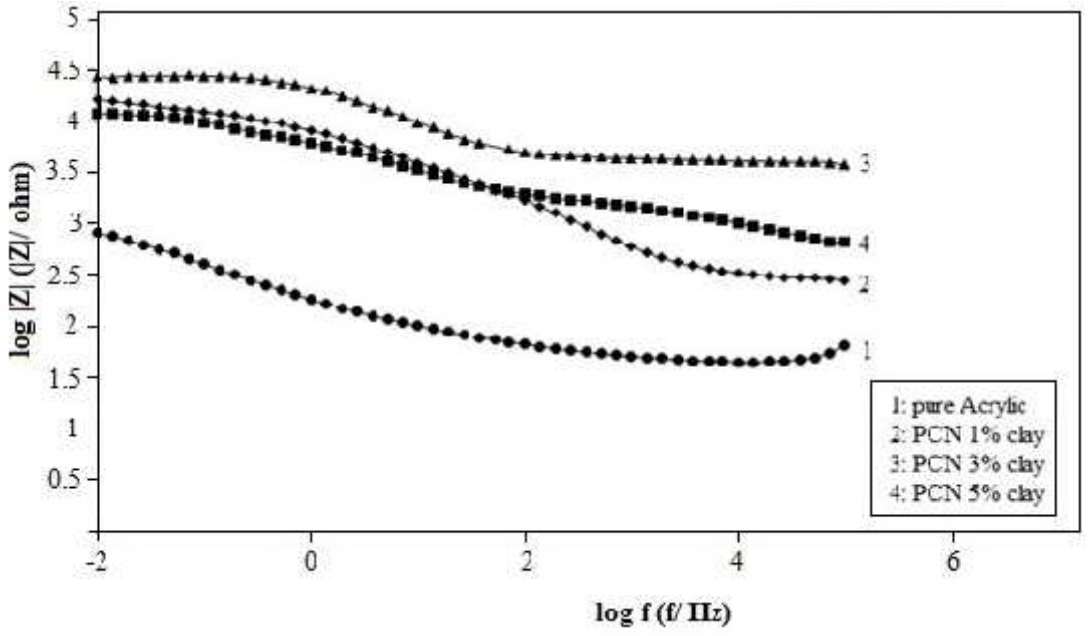

Figure 9
Bode plots of the EIS spectra for the different samples after 45 days of immersion in a 3.5 wt.% NaCl solution.

The EIS results of the nanocomposite indicated that the resistance of 3 wt.% clay nanocomposite was higher than the others in all immersion times. This meant that adding 3 wt.% clay into the acrylic matrix improved corrosion prevention, but for more than 3 wt.% clay caused an adverse effect. In fact, the free volume of polymeric matrix was higher in the neat acrylic coating than in the nanocomposite coating, so the aggressive agents can diffuse through cavity easily. The clay plates in the nanocomposite

decreased the permeation of aggressive ions and molecules into the coating by increasing the tortuous pathway (Osman et al., 2003; Mittal, 2009).

3.5.2. Tafel polarization study

To study the anticorrosive efficiency of the nanocomposite coatings, the electrochemical polarization analysis was employed. Figure 10 shows the Tafel plots for the acrylic resin and the nanocomposites with 1, 3, and 5 wt.% clay in a 3.5 wt.% NaCl solution after 45 days of immersion.

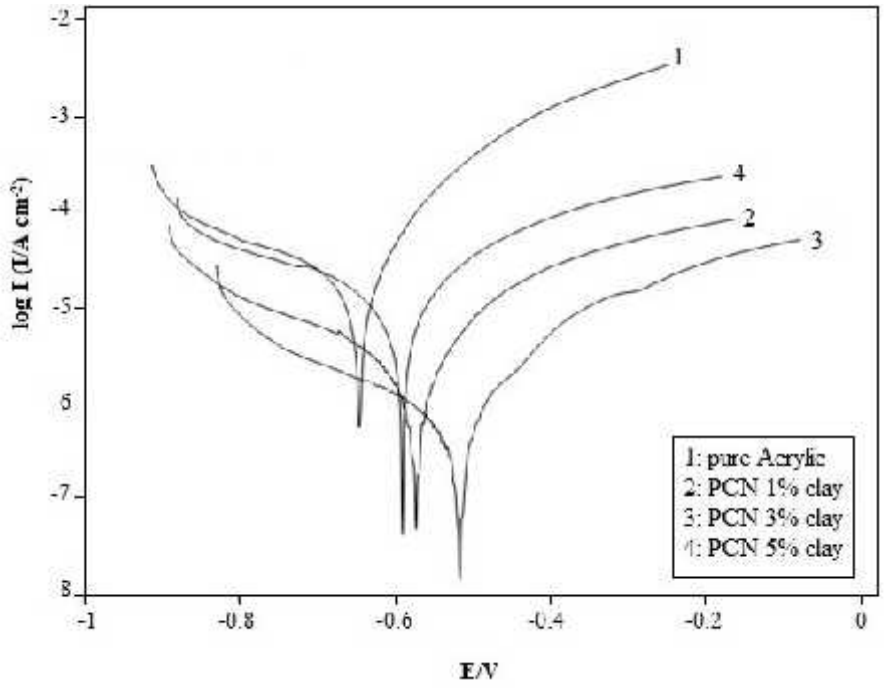

Figure 10
Polarization curves of the different samples after 30 days of immersion in a 3.5 wt.% NaCl solution.

Tafel calculations are listed in Table 3, where E_{corr}, R_p, I_{corr}, β_a, β_c, and R_{corr} represent the corrosion potential, polarization resistance, corrosion current, corrosion rate, anode Tafel constant, cathode Tafel constant, and corrosion resistance respectively.

Table 3
Electrochemical corrosion measurement of the samples after 30 days of immersion in a 3.5 wt.% NaCl solution.

Coating type	$E_{corr.}$ (V)	R_p (K t cm^2)	c (V dec^{-1})	a (V dec^{-1})	$I_{corr.}$ (μA cm^{-2})	Corrosion rate (mm per year)
pure acrylic(MP35)	-0.645	6.325	0.033	0.045	1.307	0.01535
PNC1%	-0.573	63.995	0. 034	0.04	0.1247	0.001465
PNC3%	-0.517	187.716	0.034	.043	0.04392	0.0005159
PNC5%	-0.591	14.665	0.033	0.038	0.4822	0.005664

The nanocomposite samples showed a more positive value of E_{corr}, a lower value of I_{corr}, and a higher value of R_p compared to the neat acrylic coating. It could be seen that the corrosion current of the 3 wt.% clay nanocomposite coated sample was much lower than the other coated samples and provided a better corrosion protection.

3.5.3. Salt spray test

The salt spray test was employed to evaluate the corrosion performance of the acrylic–clay nanocomposite coatings according to ASTM B-117 for 720 hrs. The photographs of the samples during 500 hrs exposing to salt spray (fog) chamber are presented in Figure 11.

ASTM D714 was employed to determine the size, density, and frequency of the blisters on the coatings. The size of the blisters was identified by numbers 2, 4, 6, and 8, where 2 and 8 represent the largest and smallest blisters respectively. The frequency of blister occurrence as the percent of surface rusting beneath or through a paint film was evaluated by using ASTM D610. The results of the salt spray test for the coated samples are shown in Table 4.

Table 4
Anticorrosive performance evaluation of the salt-spray tested coatings.

Coating type	Blisters in paint area ASTM D714	Percent of surface rusted ASTM D610
pure acrylic(MP35)	Blister size No. 4, medium	20
PNC1%	Blister size No. 6, few	0.1
PNC3%	Blister size No. 8, few	0.03
PNC5%	Blister size No. 8, few	0.03

The results showed that the degradation and blistering density of the samples were reduced by an increase in the clay concentration. The nanocomposite samples showed significantly higher corrosion resistance than the neat acrylic coating.

For the neat sample, a lot of blisters were detected on the surface, and there was rust under the blisters; for the 1 wt.% clay nanocomposite sample, some small blisters were detected on the surface. The samples containing 3 and 5 wt.% clay showed the highest corrosion resistance in the salt spray test. The enhancement of the corrosion resistance of the nanocomposite coatings may be due to the nanoclay, which filled the voids and crevices of polymeric matrix, thereby increasing the barrier properties of the coatings and improving the corrosion resistance.

3.6. Adhesion measurement

Pull-off and cross-cut adhesion tests were used to determine the strength of the bond between the substrate and coating. In the pull-off test, adhesion is measured in terms of forces used to separate the test dollies glued to the paint film from the base metal. The results of the adhesion tests before the exposure of the coated sample to a corrosive environment showed that all the samples adhered well to the substrate and the coating films did not detach from the substrate. Table 5 shows the results of the pull-off adhesion test after exposure to 720 hrs salt spray.

Table 5
Pull-off adhesion test results.

Coating type	Adhesive strength (MPa) after exposure	Ratio of the nanocomposite adhesion to the neat acrylic adhesion
Neat acrylic (Mp35)	9.1	1
PNC1%	10.5	1.154
PNC3%	10.7	1.175
PNC5%	9.7	1.066

After exposure to salt spray, the adhesion was decreased for all the samples. The decrease in the adhesion of the pure acrylic was quite significant, but it was very small for the acrylic/clay nanocomposite coatings. Moreover, the sample containing 3 wt.% clay showed the highest adhesion to the substrate.

The cross cut adhesion test was utilized to evaluate the adhesion of the coating layers applied on a substrate. The results for the cross cut adhesion tests of the coated samples before and after exposure to 720 hrs salt spray are tabulated in Table 6. Before exposure, increasing the clay in the matrix of acrylic no change was observed in the adhesion of the coatings. Because of the good dispersion and distribution of nanoclay, the coatings did not lose their adhesion to the substrate. However, after exposure to 720 hrs salt spray, the cross-cut adhesion was improved by an increase of clay up to 3 wt.%.

The samples with 1 wt.% and 3 wt.% clay showed the highest adhesion to the substrate. The decrease in adhesion was due to the penetration of water molecules and aggressive ions into the interface of the substrate and the coating, which was decreased by the incorporation of nanoclay into the acrylic matrix (Allie et al., 2008). As shown in Tables 5 and 6, after exposure, the adhesion of the coating to the substrate was increased by adding nanoclay to the coating.

Table 6
Cross-cut adhesion test results.

Sample	Grade before exposure	Grade after exposure
Neat acrylic	5B	3B
PNC1%	5B	5B
PNC3%	5B	5B
PNC5%	5B	4B

4. Conclusions

The acrylic/clay nanocomposite coatings containing various amounts of clay were prepared using a mechanical agitation and sonication process. The XRD, TEM, and optical microscopy analyses results showed that, in the cured nanocomposites, the clay particles were dispersed and intercalated. The corrosion performance of these coatings was studied using EIS measurements, polarization, salt spray, pull-off, and cross-cut adhesion tests. The results of corrosion tests showed that the addition of clay into the acrylic resin offers better barrier protection compared to the neat coatings. The 3 wt.% clay nanocomposite showed the highest corrosion protection value among the coating formulations. Finally, the samples including 1 wt.% and 3 wt.% clay showed the highest adhesion to the substrate.

References

Allie, L., Thorn, J., and Aglan, H., Evaluation of Nanosilicate Filled Poly (Vinyl Chloride-Co-Vinyl Acetate) and Epoxy Coatings, Corrosion Science., Vol. 50, No. 8, p. 2189-2196, 2008.

Ash, B. J., Rogers, D. F., Wiegand, C. J., Schadler, L. S., Siegel, R. W., Benicewicz, B. C., and Apple, T., Mechanical Properties of Al_2O_3/Poly(methyl methacrylate) Nanocomposites, Polymer Composites, Vol. 23, No. 6, p 1014-1025, 2002.

Bagherzadeh, M. R. and Mahdavi, F., Preparation Of Epoxy/Clay Nanocomposite and Investigation on its Anti-Corrosive Behavior in Epoxy Coating, Progress in Organic Coatings, Vol. 60, No. 2, p. 117-120, 2007.

Bierwagen, G. P., Reflections on Corrosion Control by Organic Coatings, Progress in Organic Coatings, Vol. 28, No. 1, p. 43-48, 1996.

Chang, K. C., Lin, H. F., Lin, C. Y., Kuo, T. H., Huang, H. H., Hsu, S. C., and Yu, Y. H., Effect of Amino-modified Silica Nanoparticles on the Corrosion Protection Properties of Epoxy Resin-Silica Hybrid Materials, Journal of Nanoscience and Nanotechnology, Vol. 8, No. 6, p. 3040-3049, 2008.

Chang, K. C., Chen, S. T., Lin, H. F., Lin, C. Y., Huang, H. H., Yeh, J. M., and Yu, Y. H., Effect of Clay on the Corrosion Protection Efficiency of PMMA/Na^+/MMT Clay Nanocomposite Coatings Evaluated by Electrochemical Measurements, European Polymer Journal, Vol. 44, No. 1, p. 13-23, 2008.

Chen-Yang, Y. W., Yang, H. C., Li, G. J., and Li, Y. K., Thermal and Anticorrosive Properties of Polyurethane/Clay Nanocomposites, Journal of Polymer Research, Vol. 11, No. 4, p. 275-283, 2005.

Chen, C., Khobaib, M., and Curliss, D., Epoxy Layered-silicate Nanocomposites, Progress in Organic Coatings, Vol. 47, No. 3, p. 376-383, 2003.

Darmiani, E., Danaee, I., Rashed, G. R., and Zaarei, D., Formulation and Study of Corrosion Prevention Behavior of Epoxy Cerium Nitrate–montmorillonite Nanocomposite Coated Carbon Steel, Journal of Coatings Technology and Research, Vol. 10, No. 4, p. 493-502, 2013.

Lan, T. and Pinnavaia, T. J., Clay-reinforced Epoxy Nanocomposites, Chemistry of Materials, Vol. 6, No. 12, p. 2216-2219, 1994.

Mittal, V, Polymer Layered Silicate Nanocomposites: A Review, Materials, Vol. 2, No. 3, p. 992-1057, 2009.

Osman, M. A., Mittal, V., Morbidelli, M., and Suter, U. W., Polyurethane Adhesive Nanocomposites as Gas Permeation Barrier, Macromolecules, Vol. 36, No. 26, p. 9851-9858, 2003.

Pavlidou, S. and Papaspyrides, C. D., A Review on Polymer–Layered Silicate Nanocomposites, Progress in Polymer Science, 33 (12) 1119-1198 (2008)

Ranade, A., D'Souza, N. A., and Gnade, B., Exfoliated and Intercalated Polyamide-imide Nanocomposites with Montmorillonite, Polymer, Vol. 43, No. 13, p. 3759-3766, 2002.

Ratna, D., Manoj, N. R., Varley, R., Singh Raman, R. K., and Simon, G. P, Clay-reinforced Epoxy Nanocomposites, Polymer International, Vol. 52, No. 9, p. 1403-1407, 2003.

Solarski, S., Benali, S., Rochery, M., Devaux, E., Alexandre, M., Monteverde, F., and Dubois, P., Synthesis of a Polyurethane/Clay Nanocomposite Used as Coating: Interactions between the Counterions of Clay and the Isocyanate and Incidence on the Nanocomposite Structure, Journal of Applied Polymer Science, Vol. 95, No. 2, p. 238-244, 2005.

Sun, Q., Schork, F. J., and Deng, Y., Water-based Polymer/Clay Nanocomposite Suspension for Improving Water and Moisture Barrier in Coating, Composites Science and Technology, Vol. 67, No. 9, p. 1823-1829, 2007.

Thi Xuan Hang, T., Truc, T. A., Nam, T. H., Oanh, V. K., Jorcin, J. B., and Pébère, N., Corrosion Protection of Carbon Steel by an Epoxy Resin Containing Organically Modified Clay, Surface and Coatings Technology, Vol. 201, No. 16, p. 7408-7415, 2007.

Xidas, P. I. and Triantafyllidis, K. S. Effect of the Type of Alkylammonium Ion Clay Modifier on the Structure and Thermal/Mechanical Properties of Glassy and Rubbery Epoxy/Clay Nanocomposites, European Polymer Journal, Vol. 46, No. 3, p. 404-417, 2010.

Xiong, J., Liu, Y., Yang, X., and Wang, X., Thermal and Mechanical Properties of Polyurethane/Montmorillonite Nanocomposites Based on a Novel Reactive Modifier, Polymer Degradation and Stability, Vol. 86, No. 3, p. 549-555, 2004.

Yeh, J. M., Liou, S. J., Lai, C. Y., Wu, P. C., and Tsai, T. Y., Enhancement of Corrosion Protection Effect in Polyaniline via the Formation of Polyaniline/Clay Nanocomposite Material, Chemistry of Materials, Vol. 13, No. 3, p. 1131-1136, 2001.

Yeh, J. M., Chin, C. P., and Chang, S., Enhanced Corrosion Protection Coatings Prepared from Soluble Electronically Conductive Polypyrrole/Clay Nanocomposite Materials, Journal Applied Polymer Science, Vol. 88, No. 14, p. 3264-3272, 2003.

Yeh, J. M., Liou, S. J., Lin, C. Y., Cheng, C. Y., Chang, Y. W., and Lee, K. R., Anticorrosively Enhanced PMMA/Clay Nanocomposite Materials with Quaternary Alkylphosphonium Salt as an Intercalating Agen, Chemistry of Materials, Vol. 14, No. 1, p. 154-161, 2002.

Yeh, J. M., Liou, S. J., Lin, C. G., Chang, Y. P., Yu, Y. H., and Cheng, C. F., Effective Enhancement of Anticorrosive Properties of Polystyrene by Polystyrene/Clay Nanocomposite Materials, Journal Applied Polymer Science, Vol. 92, No. 3, p. 1970-1976, 2004.

Yu, Y. H., Yeh, J. M., Liou, S. J., and Chang, Y. P., Organo-soluble Polyimide (TBAPP–OPDA)/Clay Nanocomposite Materials with Advanced Anticorrosive Properties Prepared from Solution Dispersion Technique, Acta Materialia, Vol. 52, No. 2, p. 475-486, 2004.

Zaarei, D., Sarabi, A. A., Sharif, F., and Kassiriha, S. M., Structure, Properties, and Corrosion Resistivity of Polymeric Nanocomposite Coatings Based on Layered Silicates, Journal of Coatings Technology and Research, Vol. 5, No. 2, p. 241-249, 2008.

Zaarei, D., Sarabi, A. A., Sharif, F., Gudarzi, M. M., and Kassiriha, S. M., The Impact of Organoclay on the Physical and Mechanical Properties of Epoxy/Clay Nanocomposite Coatings, Journal of Macromolecular Science Part B, Vol. 49, No. 5, p. 960-969, 2010.

Zhang, S., Sun, D., Fu, Y., and Du, H., Recent Advances of Super hard Nanocomposite Coatings: A Review, Surface and Coatings Technology, Vol. 167, No. 2, p. 113-119, 2003.

Zhou, S., Wu, L., Sun, J., and Shen, W., The Change of the Properties of Acrylic-based Polyurethane via Addition of Nanosilica, Progress in Organic Coatings, Vol. 45, No.1, p. 33-42, 2002.